Nanocrystalline hydroxyapatite doped with aluminium: A potential carrier for biomedical applications

Tanaji V. Kolekar[a,b,*], Nanasaheb D. Thorat[c], Hemraj M. Yadav[d], Veeresh T. Magalad[a,e,*], Mahesh A. Shinde[b], Sneha S. Bandgar[f], Jin H. Kim[g], Ganesh L. Agawane[h]

Abstract

Biocompatible materials based on hydroxyapatite are potentially attractive for a wide range of medical applications. The effect of aluminium substitution on the biocompatibility of hydroxyapatite (HA) under the physiochemical conditions has been investigated. Various samples of aluminium doped hydroxyapatite (Al-HA) with different concentration (0, 0.5, 1.0, 1.5, 2.0, 2.5 mol%) were successfully synthesised by solution combustion method and characterized by X-ray Diffraction (XRD), Transmission Electron Microscopy (TEM), and Scanning Electron Microscopy (SEM), and thermal analysis technique. XRD and TEM results reveal uniform and crystalline nature of Al-HA nanoparticles. The biocompatibility of the Al-HA nanoparticles was studied using L929 cell lines by MTT assays up to 24 h. These Al-HA nanoparticles are biocompatible on cell lines L929 and do not have toxic effects for further possible *in vivo* applications. The results of these studies confirmed the biocompatibility of Al-HA and demonstrated the suitability for biomedical applications. The present work reveals the importance of structural, morphological, biocompatible properties of Al-HA nanoparticles and predicts the suitability for biomedical applications.

Keywords: Sol–gel processes; Nanocomposites; Apatite; Biomedical applications

1. Introduction

Calcium orthophosphate based inorganic biomaterials have a wide range of biomedical applications [1,2]. Among them, hydroxyapatite (HA) is one of the most promising inorganic biomaterials. HA is the principal mineral constituents of natural bones and teeth [3]. The bioactive ceramics HA [$Ca_{10}(PO_4)_6(OH)_2$] is able to bond with living tissues and one of the most attractive calcium phosphates due to its medical applications. HA has become one of the most important bioceramic materials for artificial bone owning to its excellent biocompatibility and surface active properties with living tissues [4,5]. Since 1980, HA has been commercially used as a coating on metallic implants. An ideal bone implant should be osteoinductive, resorbable and easy to shape, and possessing adequate mechanical properties. Therefore, artificial HA is widely applicable in the field of bone tissue engineering [6,7]. Restoration of loosed bone, maxillofacial reconstruction, spinal surgery and bone repair after tumour surgery are some applications of HA in orthopaedics and dentistry [8–10]. Recent research reported that HA nanoparticles can retard the

*Corresponding authors at: VTU Research Resource Centre, Visvesvaraya Technological University, Belagavi 590018, Karnataka, India.
Fax: +91 831 2405467.
E-mail addresses: rhts.kolekar@gmail.com (T.V. Kolekar), magaladvt@gmail.com (V.T. Magalad).

http://dx.doi.org/10.1016/j.ceramint.2015.12.060
0272-8842/

growth of cancer cells [11]. However, synthetic pure HA has certain inferior properties such as poor mechanical properties, a high degree of crystallinity and higher structural stability. This results in a low rate of biodegradation causing a poor response as an orthopaedic implant material [12–14].

Metal doping in HA for biomedical applications has gained lot of attention because of the high stability and flexibility of apatite structure, a great number of cationic substitution area of potential application in the biomedical field [15–17]. The HA structure is so tolerant to ionic substitutions hence, Ca sites can be replaced by various divalent (Ca^{2+} Mg^{2+},Sr^{2+},Cd^{2+}, Pb^{2+} and Ba^{2+}) [18–24] and trivalent cations (Al^{3+},Fe^{3+}) [25]. It is well known that metal ions doping in HA can influence the biomedical properties of the HA by improving its biocompatibility. Replacement of Ca ions by other cations can lead to contraction or expansion of the lattice parameters, depending upon ionic size. Copper and zinc-doped HA nanomaterials exhibited viable cells reduction ability for a for a wide range of microorganisms [26].

The synthetic HA is not suitable for bone implant in load bearing applications, due to its lack of strength and brittleness. In addition to this, a high degree of crystallinity results in reduced degradability of pure HA when it is implanted into the organ [27]. In order to overcome these limitations, HA is doped with various metals such as strontium [28], manganese [29], magnesium[30,31], titanium [32] and zinc [33] to improve its mechanical strength. It is reported that minerals and traces of metal elements accelerate bone formation and resorption on bone cells *in vivo* and *in-vitro* [28,34].

HA is associated with minor groups and elements (e.g. CO_3^{2-}, HPO_4^{2-}, Na, Mg^{2+}) and trace elements (e.g. Sr^{2+}, K^+, Cl^-, $Al^{3+}$and F^-), some of them at mg L^{-1} level [35]. A bio inert ceramics such as alumina is used as load-bearing articulating material specifically designed with mechanical and biocompatible properties. [36].

The synthesis of HA have been carried out using various methods such as sol–gel process [2], emulsion and micro-emulsion [37], co-precipitation [38], microwave irradiation [39], etc. The nanoparticles obtained from sol–gel method generally contains sol–gel matrix components at the surfaces of particles which alter the structural and magnetic properties of the material [40]. The combustion technique has also been employed for the synthesis of HA nanoparticles in the biomedical field to overcome the disadvantages mentioned above [38]. Short duration process and the formation of various gases during combustion inhibits particle size growth and favours the synthesis of nanosize materials with the high specific surface area.

In the present investigation, nanocrystalline HA was prepared by a facile combustion method. This work aims to study the effect of aluminium on the bioactivity of nanocrystalline HA under the physiological conditions. The cytotoxicity assessments have been carried out to evaluate the biocompatibility of nanocrystalline HA and Al-HA with different concentration. Cytotoxicity of the prepared material has been studied by utilising L929 (mouse Fibroblast) cell line for 12 and 24 h. For this, trypan blue dye exclusion (TBDE) and MTT assays were performed to identify the possible toxicity of nanoparticles.

2. Experimental

2.1. Materials

Calcium nitrate tetrahydrate and *di*-Ammonium hydrogen orthophosphate were purchased from Sigma-Aldrich and aluminium nitrate were purchased from Thomas Baker. All chemicals used here were of analytical grade and used without further purification.

2.2. Synthesis of Al-doped hydroxyapatite

Al-doped hydroxyapatite (Al-HA) with different concentration (0, 0.5, 1.0, 1.5, 2.0, 2.5 mol%) were prepared by modifying solution combustion method reported previously [41]. For this, polyvinyl alcohol (PVA) was used as a fuel. In brief, the stoichiometric amounts of the nitrate precursors Ca $(NO_3)_2{\cdot}4H_2O$, Al $(NO_3)_3{\cdot}9H_2O$ and phosphate precursor $(NH_4)_2HPO_4$ were dissolved in double distilled water to form the solution of 0.1 M. The equimolar solution of PVA was prepared in double distilled water. The mixture of oxidants and fuel was placed onto a magnetic stirrer for 30 mins to get uniform mixing. Evaporation of water to form a gel of precursors was carried out at 100 °C and then the gel was heated at 300 °C to obtain a powder. The obtained powder of Al-HA was then annealed at 950 °C for 6 h to remove carbon residues and then used for further analysis. The dried mixture possesses the characteristics of combustion and can be ignited to start combustion reaction using muffle furnace. Various Al-doped hydroxyapatite samples containing Al content 0, 0.5, 1.0, 1.5, 2.0, 2.5 mol % were denoted as HA, Al-HA-1, Al-HA-2, Al-HA-3, Al-HA-4, Al-HA-5, respectively.

2.3. Characterisations

2.3.1. Structural and morphological studies

The structural and morphological studies of the samples were studied using X-ray Diffractometer (XRD), Fourier Transform Infrared spectroscopy (FTIR), Transmission Electron Microscopy (TEM) and Scanning Electron Microscopy. Phase identification and structural analysis of Al-HA were studied using X-ray diffraction (Philip-3710) with Cu-Kα radiation in the 2θ range from 10° to 80°. The pattern were analysed by X-pert high score plus software and compared with the Joint Committee on Powder Diffraction Standards (JCPDS) (JCDPS card no. 01-074-0565 and 01-075-0278). The surface morphology and particles sizes of the Al-HA were determined by using transmission electron microscope (Philips CM 200 model) with an operating voltage of 20–200 kV and a resolution of 2.4 Å. The compositional analysis was done by energy dispersive spectroscopy (EDS, JEOL JSM 6360). A Perkin-Elmer spectrometer (Model no. 783 USA) was used to obtain FTIR spectra of Al-HA samples in the range of 450 to 4000 cm^{-1} using KBr pellets.

2.4. Biocompatibility study

2.4.1. Cell culture

In vitro cytotoxicity of nanocrystalline Al-HA was carried out by using MTT assay on L929 (mouse fibroblast) cell lines obtained from National Centre for Cell Sciences, Pune (India) while toxicity study was carried out at National Toxicology Centre Pune (ISO 10993/USP 32 NF 27). The L929 cells were grown in DMEM (Dulbecco's modified Eagle's medium) supplemented with 10% (v/v) foetal bovine serum, kanamycin (0.1 mg/mL), penicillin G (100 U/mL), and sodium bicarbonate (1.5 mg mL^{-1}) at 37 °C in a 5% CO_2 atmosphere. MTT assays were used for cytotoxicity study.

2.4.2. MTT assay

The details of MTT assay to test cytotoxicity of various nanomaterials have been reported in our recent reports [41–43]. In brief, the L929 cells were incubated with the concentration of 2×10^5 cells mL^{-1} in the respective medium for 24 h in a 96-well microtiter plate. After 24 h, the old media was replaced by fresh media and different proportions of sterile Al-HA (0.01, 0.05, 0.1, 0.2, 0.4, 0.6, 0.8 and 1 mg/mL of culture media). Then the total medium was incubated at 37 °C in a 5% CO_2 atmosphere for 12 and 24 h. After 12 and 24 h, the 10 μL MTT solution was added into each well including control wells. The plates were incubated for 3 h at 37 °C in a 5% CO_2 atmosphere for metabolization of MTT with the nanoparticles and cell media. Then the total medium was removed by flicking the plates and only anchored cells remained in the wells. The cells were then washed with PBS and formed formazan was extracted in 200 μL acidic isopropanol. Finally, absorbance was recorded at 570 nm and the cell viability was calculated. The experiments were replicated three times and the data was graphically presented as mean ± SD. The relative cell viability (%) compared with control well containing cells without nanoparticles are calculated by the equation:

$$\text{Relative cell viability}(\%) = [A_{absorbance}]_{tested} / [A_{absorbance}]_{control} \times 100 \cdot \quad (1)$$

3. Results and discussion

3.1. Thermogravimetric analysis

TGA curve of pure HA and the representative Al-HA-5 are shown in Fig. 1. In TGA curve, four different stages were observed during the total weight loss. The first stage of weight loss is in between room temperature to 230 °C, which is due to the loss of physically adsorbed water. The second stage of weight loss is from 230 to 430 °C and this is due to loss of chemisorbed water, organic groups and solvent attached to the sample. The third stage is from 430 to 830 °C, and above 830 °C the weight loss is less than 0.65%. Taking into consideration of TGA studies, all the samples are calcinated at 950 °C for their further characterisation.

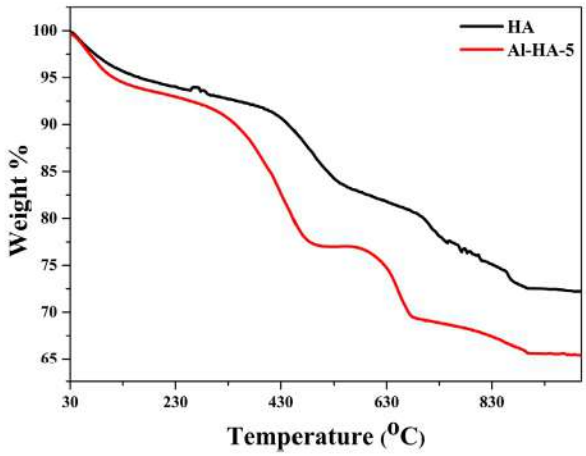

Fig. 1. TGA pattern of pure HA and HA-Al-5 nanoparticles.

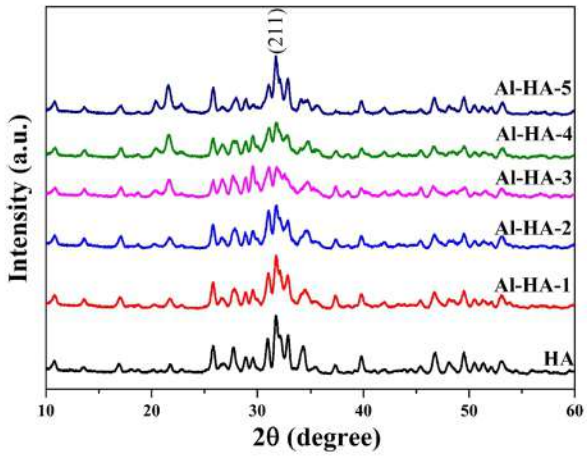

Fig. 2. XRD patterns of pure HA and Al-HA nanoparticles.

3.2. XRD analysis

XRD patterns of the pure HA and Al-HA samples are shown in Fig. 2. The main phase in all samples was identified as hydroxyapatite (JCDPS no. 01-074-0565) while the secondary phases of Al (JCDPS no. 01-083-2081) was observed for doped samples with small extent. HA showing a hexagonal structure with space group $P6_3/m$. It can be seen that, the lattice parameters of the prepared samples are in excellent agreement with standard data $a=9.4240$ Å, $c=6.8790$ Å and $a=4.7180$ Å, $c=12.8180$ Å for HA and Al-HA, respectively. Gaussian fit of the most intense peak (211) was used to calculate the full width at half maxima for the determination of crystallite size (D) by using the Scherrer equation:

$$D = \frac{0.9\lambda}{\beta \cos\theta} \quad (2)$$

where D is the crystallite size, λ is the wavelength of Cu-Kα radiations ($\lambda=1.5405$ Å), θ is the corresponding Braggs diffraction angle and β is full width at half maxima of the most intense peak (211). The average crystallite sizes of HA and Al-HA were found to be 34.50 nm and 32.42 nm, respectively.

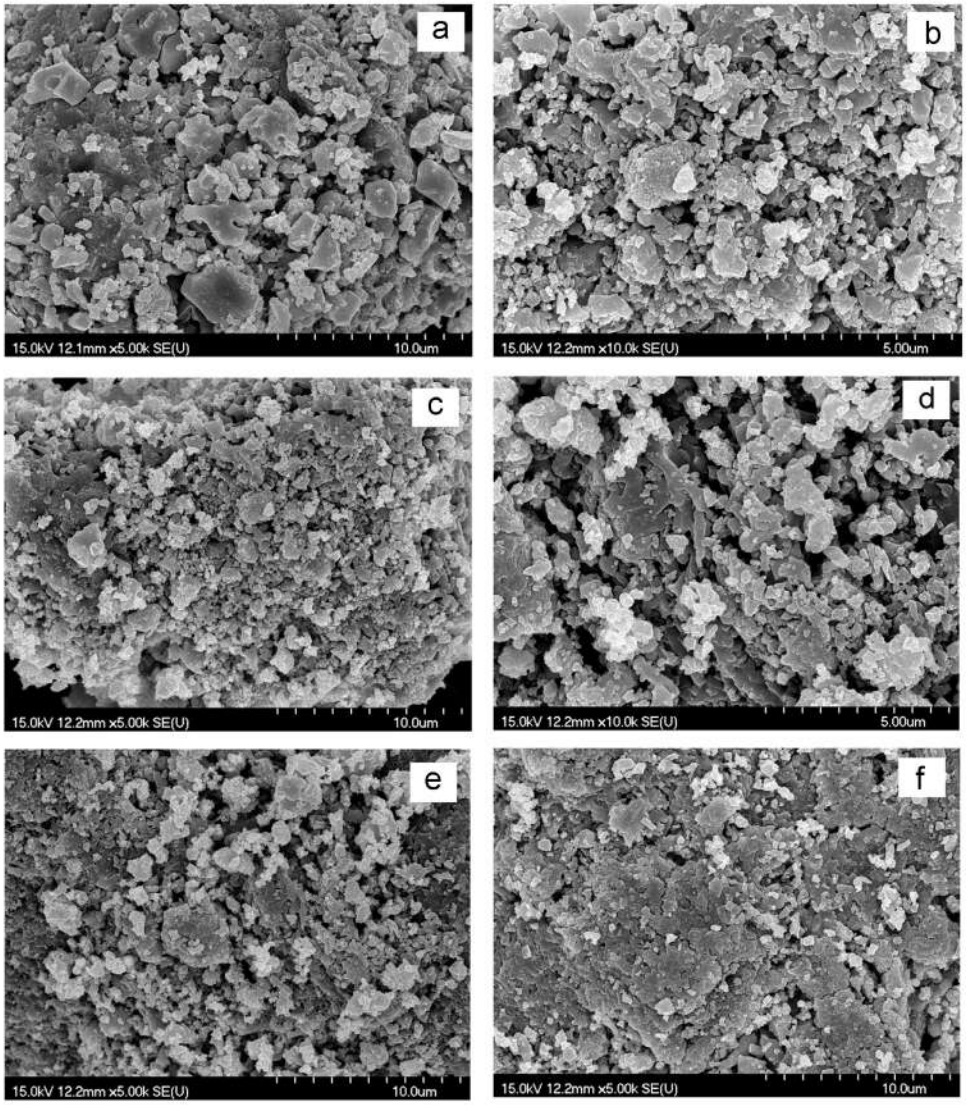

Fig. 3. SEM images of (a) pure HA, (b) Al-HA-1, (c) Al-HA-2, (d) Al-HA-3, (e) Al-HA-4, and (f) Al-HA-5.

3.3. SEM analysis

SEM technique was used to observe and analyse the microstructure, agglomeration and grain sizes of Al-HA. SEM micrographs of HA and Al-HA samples are depicted in Fig. 3. SEM micrographs of samples are shown similar agglomerates that are consisting of fine crystallites and small size. It has been reported that crystal size distribution of bone plays an important role in bone fracture [37].

The EDS spectra was used for quantitative elemental analysis of the HA and Al-HA samples. Fig. 4 shows EDS spectra of HA and a representative Al-HA sample. The EDS spectra indicate that samples are consistent with their elemental signals and stoichiometry is as expected. In the case of pure HA, the corresponding peaks are due to the presence of calcium (Ca), phosphor (P), and oxygen (O) while for Al-HA samples the observed peaks corresponds with aluminium (Al), calcium (Ca), phosphor (P), oxygen (O). This implies that the prepared samples are pure in nature. The elemental composition estimated from EDS analysis is tabulated in Table 1.

The Ca/P atomic ratios for pure HA is 1.66 which is in close agreement with the standard 1.67. The Ca/P atomic ratios (1.47, 1.49, 1.45.1.42, 1.38) for Al-HA samples are little smaller than that of the standard. It is observed that there is a decrease in Ca/P atomic ratio in the Al-HA samples. This can be attributed due to the proper substitution of Ca with metal ion during the preparation process. The larger multivalent ions can be effectively removed than smaller ions [44]. It has been found that Ca deficient apatite (Ca/P atomic ratios between 1.33 & 1.55) could be very beneficial to the formation of new bone *in vivo* [45]. Thus, Al-doped HA could be beneficial for the formation of new bone *in vivo*.

3.4. TEM analysis

The particles size of HA and Al-HA were estimated from TEM analysis. Fig. 5 shows TEM micrographs of HA and Al-HA-5. The HA nanoparticles were a cylindrical rod-like shape with homogeneous microstructure, around 100 nm in diameter and several particles seem to aggregates. However, the particle

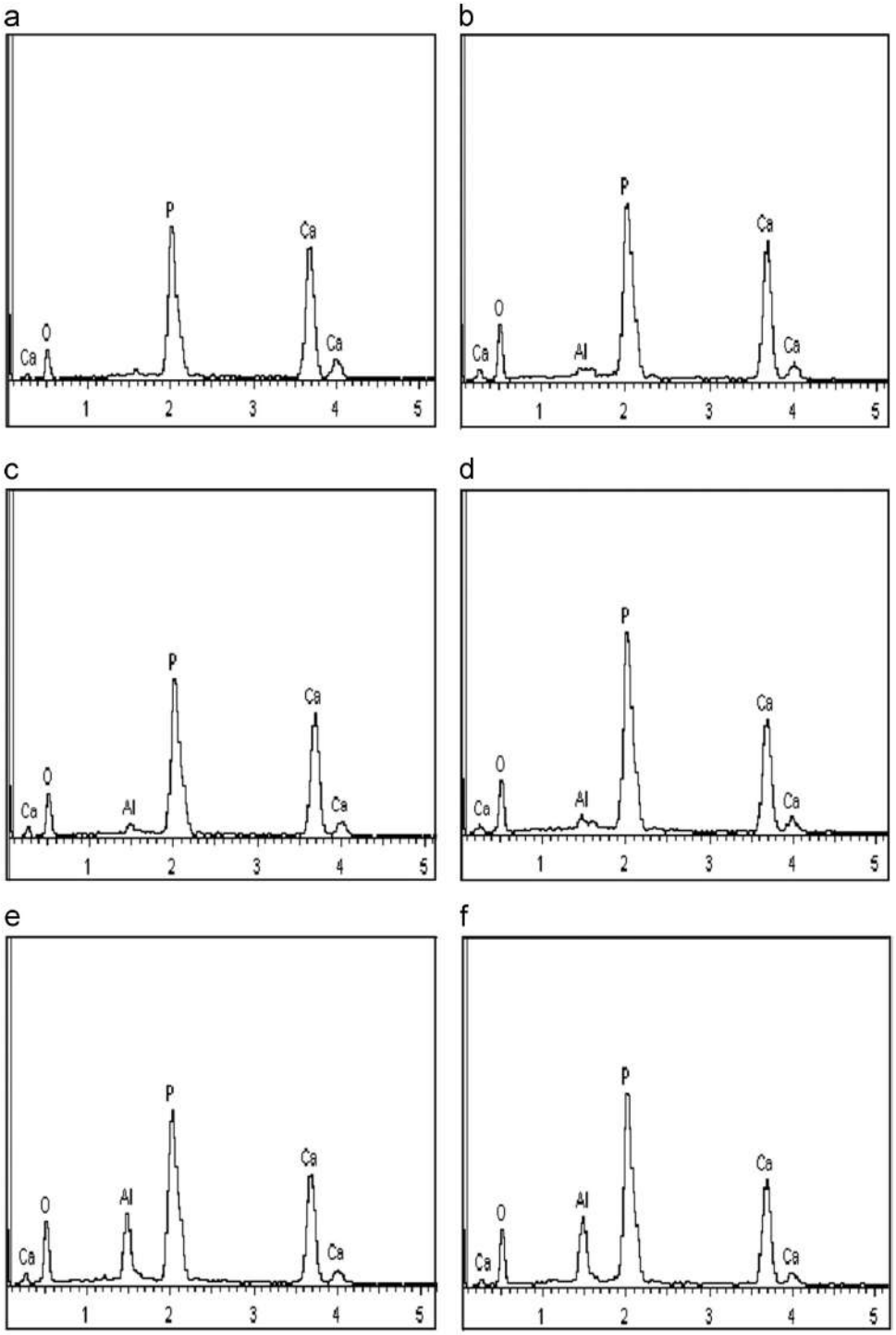

Fig. 4. EDS spectrum of (a) pure HA, (b) Al-HA-1, (c) Al-HA-2, (d) Al-HA-3, (e) Al-HA-4, and (f) Al-HA-5.

sizes of Al-HA-5 were found to be in the range of 100 nm and decreased significantly with the existence of Al element. The diameters of particles are slightly larger than the observed crystallite sizes calculated from XRD, due to the presence of noncrystalline surface layers as well as high calcination temperature (950 °C) which causes the grain growth. The corresponding SAED pattern (inset of Fig. 5(a) and (b)) shows bright ring patterns indicating the polycrystalline nature of nanoparticles which is in good agreement with XRD results.

3.5. Cytotoxicity Study

The cytotoxicity study of HA and Al-HA nanoparticles were carried out on L929 cell lines with different concentrations and with varying incubation time. The obtained data is depicted in Fig. 6(a–d). The L929 cell lines were incubated with HA, Al-HA-1, Al-HA-3, Al-HA-5 nanoparticles for 12 h and 24 h, respectively with the concentration of 0.2, 0.4, 0.6, 0.8, and 1 mg mL^{-1} at 37 °C in a 5% CO_2 atmosphere. The relative

cell viability (%) compared with a control well containing cells without nanoparticles are calculated by the equation:

$$\text{Relative cell viability}(\%) = [A]_{tested}/[A]_{control} \times 100 \cdot \quad (3)$$

The cell cytotoxicity study of HA and Ag-HA against L929 cell lines for 24 h reported by Shi et al. [46] and they found that OD values directly proportional to cell viability with regard to the concentration of nanoparticles (50–1000 μg/mL) and very low cell viability of nanoparticles on cells. In the present study, we have evaluated cytotoxicity of developed composite scaffold on L929 cells and study confirm non-toxicity behaviour on the L929 cells after 24 h incubation and reveals excellent cytocompatibility (Fig.6a–d). The low extract concentration up to 25% show very less cytotoxicity, whereas higher extract concentration induces slight toxic effect to L929 cells compared to positive control [47,48]. From cell cytotoxicity data, it was found that the cell viability gradually decreases with increasing concentration and incubation time of nanoparticles in all four samples. The reported study indicates that cytotoxicity may increase with decreasing the grain sizes since the cellular inflammatory reaction is generally enhanced by endocytosis when the particle size decreases in the range of 100 nm [49]. As compared with the previous study, the result obtained in the present investigation clearly show very low cytotoxicity on L929 cell lines.

Metanawin *et al*. reported that when any healthy cells are treated with the nanoparticles, the presence of nanoparticles on the cell surface affects the plasma membrane (not directly microtubule or nucleus of the cell) over a period of time and causes the lysis of the cell. After the removing of nanoparticles from the cell surface, cells are stained with MTT (3-(4,5-dimethylthiazol-2yl)-2,5-diphenyltetrazolium bromide). The MTT enters the cell and passes into the mitochondria where it is reduced to an insoluble, coloured (dark purple) formazan product because viable cells reduce the yellow tetrazolium salt to a blue/purple dye [50]. The cells are then solubilized with an organic solvent (e.g. isopropanol) and the released solubilized formazan is measured spectrophotometrically. Since the reduction of MTT can only occur in metabolic active cells, the level of activity is a measure of the viability of the cells.

Two factors should play important roles for the cell viability. One is the grain size and the other is their chemical stability. The particle intake by the cells is indirectly proportional to its size; as compared to larger size particles the lower size particles have an efficient interfacial interaction with the cell membrane. The sizes of nanoparticles no longer play an influencing key role in the cytotoxicity and there may be a limit beyond that cytotoxicity of the nanoparticles which is not influenced by its size. The Al-HA nanoparticles were smaller in size compared to pure HA nanoparticles hence significantly low cytotoxicity was observed. It is obvious due to the two reasons, (i) small size particles have smaller mass concentration and total surface area than the large particles and (ii) the effective interaction area of large nanoparticles on the cell is always greater than the small particles. Thus, the large particles exert a stronger stimulus on the cell surface and results in the reduction of cell viability [51,52].

From the biocompatibility study, it can be seen that there was no drastic change in the cytotoxicity of HA and Al-HA nanoparticles. This is attributed to a relatively small difference in the particle size with the change composition (Ca/P ratio). The results obtained from cytotoxicity experiments show better biocompatibility of pure-HA and Al-HA nanoparticles with a concentration up to 1 mg mL^{-1}. The preliminary cytotoxicity study on L929 cells of HA and Al-HA nanoparticles synthesised by solution combustion technique, here confirmed that

Table 1
Elemental composition of HA and Al-HA nanoparticles.

Sample	Atomic % composition			
	Al	Ca	P	O
HA	–	32.33	19.52	48.15
Al-HA-1	0.92	28.13	19.03	51.92
Al-HA-2	1.95	26.09	17.47	54.49
Al-HA-3	3.27	23.12	15.93	57.68
Al-HA-4	4.48	21.90	15.33	58.29
Al-HA-5	6.07	19.61	14.11	60.21

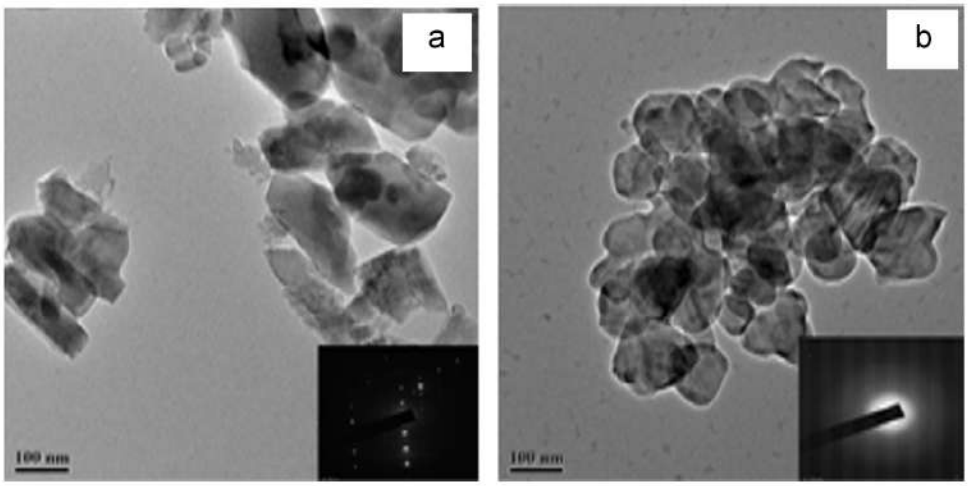

Fig. 5. TEM images of (a) HA, (b) Al-HA-5. (Inset: corresponding SAED pattern.).

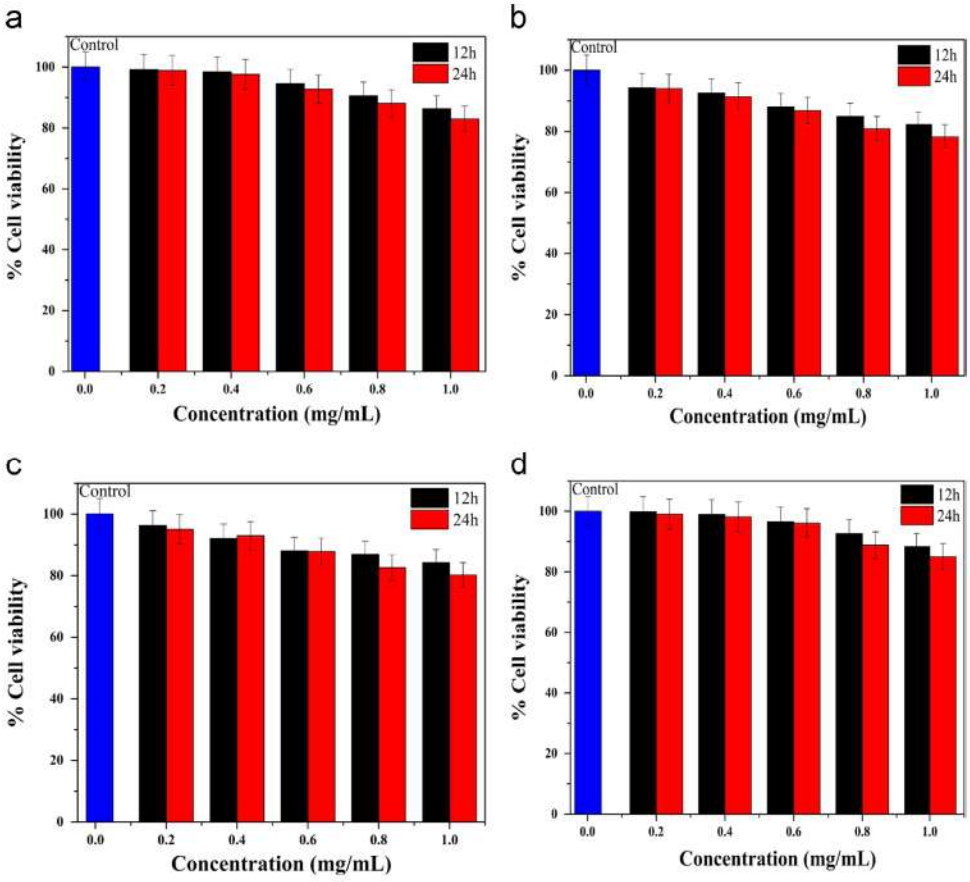

Fig. 6. Cytotoxicity profiles of (a) pure HA, (b) Al-HA1, (c) Al-HA3, (d) Al-HA-5 for 12 and 24 h.

the biological effects are not based on chemical composition alone, in addition, size, shape, aggregation state and surface texture also play an important role.

4. Conclusion

The structural and cytotoxic properties of the pure HA and Al-HA nanoparticles with different stoichiometric ratios prepared by a modified solution combustion technique have been studied in great detail. The physicochemical properties of the pure HA have been affected with the existence of aluminium. The pure HA and Al-HA nanoparticles having pure phase and almost identical particle sizes. EDS analysis confirmed the presence of pure HA and Al-HA with stoichiometric ratio and this material could be applicable for the formation of new bone *in vivo*. The cytotoxicity study established biocompatibility of nanoparticles up to 1 mg mL^{-1} and the cell viability was influenced with particle sizes. The preliminary results obtained from cytotoxicity study are highly encouraging. The results of this work demonstrate the applicability of Al-HA nanoparticles in the biomedical field. Furthermore, the cytotoxicity studies show that the Al_5-Hap lower cytotoxicity. Hence, it is revealed that Al-HA is an excellent candidate in the biomedical field.

References

[1] S.V. Dorozhkin, Calcium Orthophosphates in Nature, Biology and Medicine, Materials, Basel, 2009, p. 399–498.
[2] A. Bigi, E. Boanini, K. Rubini, Hydroxyapatite gels and nanocrystals prepared through a sol–gel process, J. Solid State Chem. 177 (2004) 3092–3098.
[3] H. Qiu, J. Yang, P. Kodali, J. Koh, G.A. Ameer, A citric acid-based hydroxyapatite composite for orthopedic implants, Biomaterials 27 (2006) 5845–5854.
[4] T. Hayakawa, M. Yoshinari, H. Kiba, H. Yamamoto, K. Nemoto, J.A. Jansen, Trabecular bone response to surface roughened and calcium phosphate (Ca–P) coated titanium implants, Biomaterials 23 (2002) 1025–1031.
[5] S.I. Roohani-Esfahani, S. Nouri-Khorasani, Z.F. Lu, M.H. Fathi, M. Razavi, R.C. Appleyard, et al., Modification of porous calcium phosphate surfaces with different geometries of bioactive glass nanoparticles, Mater. Sci. Eng. C 32 (2012) 830–839.
[6] H. Zhou, J. Lee, Nanoscale hydroxyapatite particles for bone tissue engineering, Acta Biomater. 7 (2011) 2769–2781.
[7] C.J. Chung, R.T. Su, H.J. Chu, H.T. Chen, H.K. Tsou, J.L. He, Plasma electrolytic oxidation of titanium and improvement in osseointegration, J. Biomed. Mater. Res. B. Appl. Biomater. 101 (2013) 1023–1030.
[8] L.L. Hench, Bioceramics: from concept to clinic, J. Am. Ceram. Soc. 74 (1991) 1487–1510.
[9] J. Chevalier, L. Gremillard, Ceramics for medical applications: a picture for the next 20 years, J. Eur. Ceram. Soc. 29 (2009) 1245–1255.
[10] J.A. Juhasz, S.M. Best, Bioactive ceramics: processing, structures and properties, J. Mater. Sci. 47 (2011) 610–624.
[11] A. Boskey, Bone mineral crystal size, Osteoporos. Int., 14, 2003, 16-21.
[12] C.M. Mardziah, I. Sopyan, S. Ramesh, Strontium-doped hydroxyapatite nanopowder via sol-gel method: effect of strontium concentration and

calcination temperature on phase behavior, trends biomater, Artif. Organs 23 (2009).
[13] L. Cao, C. Zhang, J. Huang, Synthesis of hydroxyapatite nanoparticles in ultrasonic precipitation, Ceram. Int. 31 (2005) 1041–1044.
[14] D. Gopi, S. Nithiya, L. Kavitha, J.M.F. Ferreira, Amino acid-assisted synthesis of strontium hydroxyapatite bone cement by a soft solution freezing method, Bull. Mater. Sci. 35 (2012) 1195–1199.
[15] Y. Matsumura, S. Sugiyama, H. Hayashi, J.B. Moffat, Lead–calcium hydroxyapatite: cation effects in the oxidative coupling of methane, J. Solid State Chem. 114 (1995) 138–145.
[16] E. Boanini, P. Torricelli, M. Gazzano, R. Giardino, A. Bigi, Alendronate-hydroxyapatite nanocomposites and their interaction with osteoclasts and osteoblast-like cells, Biomaterials 29 (2008) 790–796.
[17] X. Chen, T. Wu, Q. Wang, J.W. Shen, Shield effect of silicate on adsorption of proteins onto silicon-doped hydroxyapatite (100) surface, Biomaterials 29 (2008) 2423–2432.
[18] R.Z. LeGeros, Calcium phosphates in oral biology and medicine, Monogr. Oral. Sci. 15 (1990) 1–201.
[19] C.J. Kleber, M.S. Putt, Aluminum uptake and inhibition of enamel dissolution by sequential treatments with aluminum solutions, Caries Res. 28 (1994) 401–405.
[20] A. Yasukawa, S. Ouchi, K. Kandori, T. Ishikawa, Preparation and characterization of magnesium-calcium hydroxyapatites, J. Mater. Chem. 6 (1996) 1401–1405.
[21] T. Ishikawa, H. Saito, A. Yasukawa, K. Kandori, Adsorption of CO_2 on non-stoichiometric strontium-calcium hydroxyapatites, J. Chem. Soc. Faraday Trans. 89 (1993) 3821.
[22] A. Yasukawa, M. Higashijima, K. Kandori, T. Ishikawa, Preparation and characterization of cadmium–calcium hydroxyapatite solid solution particles, Colloids Surfaces A Physicochem. Eng. Asp. 268 (2005) 111–117.
[23] A. Yasukawa, K. Kamiuchi, T. Yokoyama, T. Ishikawa, Preparation of lead–calcium hydroxyapatite solid solutions by a wet method using acetamide, J. Solid State Chem. 163 (2002) 27–32.
[24] A. Yasukawa, E. Ueda, K. Kandori, T. Ishikawa, Preparation and characterization of carbonated barium–calcium hydroxyapatite solid solutions, J. Colloid Interface Sci. 288 (2005) 468–474.
[25] M. Wakamura, K. Kandori, T. Ishikawa, Surface structure and composition of calcium hydroxyapatites substituted with Al(III), La(III) and Fe (III) ions, Colloids Surfaces A Physicochem. Eng. Asp. 164 (2000) 297–305.
[26] V. Stanić, S. Dimitrijević, J. Antić-Stanković, M. Mitrić, B. Jokić, I.B. Plećaš, et al., Synthesis, characterization and antimicrobial activity of copper and zinc-doped hydroxyapatite nanopowders, Appl. Surf. Sci. 256 (2010) 6083–6089.
[27] N. Zahra, M. Fayyaz, W. Iqbal, M. Irfan, S. Alam, A process for the development of strontium hydroxyapatite, IOP Conf. Series Mater. Sci. Eng. 60 (2014) 012056.
[28] H.W. Kim, Y.H. Koh, Y.M. Kong, J.G. Kang, H.E. Kim, Strontium substituted calcium phosphate biphasic ceramics obtained by a powder precipitation method, J. Mater. Sci. Mater. Med. 15 (2004) 1129–1134.
[29] W. Acchar, E.G. Ramalho, Effect of MnO_2 addition on sintering behavior of tricalcium phosphate: preliminary results, Mater. Sci. Eng. C 28 (2008) 248–252.
[30] S. Kannan, I.A.F. Lemos, J.H.G. Rocha, J.M.F. Ferreira, Synthesis and characterization of magnesium substituted biphasic mixtures of controlled hydroxyapatite/β-tricalcium phosphate ratios, J. Solid State Chem. 178 (2005) 3190–3196.
[31] E. Landi, A. Tampieri, M. Mattioli-Belmonte, G. Celotti, M. Sandri, A. Gigante, et al., Biomimetic Mg- and Mg, CO3-substituted hydroxyapatites: synthesis characterization and in vitro behaviour, J. Eur. Ceram. Soc. 26 (2006) 2593–2601.
[32] K. Niespodziana, K. Jurczyk, J. Jakubowicz, M. Jurczyk, Fabrication and properties of titanium–hydroxyapatite nanocomposites, Mater. Chem. Phys. 123 (2010) 160–165.
[33] M. Li, X. Xiao, R. Liu, C. Chen, L. Huang, Structural characterization of zinc-substituted hydroxyapatite prepared by hydrothermal method, J. Mater. Sci. Mater. Med. 19 (2008) 797–803.
[34] A. Bigi, E. Boanini, C. Capuccini, M. Gazzano, Strontium-substituted hydroxyapatite nanocrystals, Inorganica Chim. Acta 360 (2007) 1009–1016.
[35] H.C.W. Skinner, Biominerals, Miner. Mag. 69 (2005) 621–641.
[36] S. Bodhak, S. Nath, B. Basu, Friction and wear properties of novel HDPE–HAp–Al2O3 biocomposites against alumina counterface, J. Biomater. Appl. 23 (2008) 407–433.
[37] M.J. Phillips, J.A. Darr, Z.B. Luklinska, I. Rehman, Synthesis and characterization of nano-biomaterials with potential osteological applications, J. Mater. Sci. Mater. Med. 14 (2003) 875–882.
[38] S. Kannan, A.F. Lemos, J.M.F. Ferreira, Synthesis and mechanical performance of biological-like hydroxyapatites, Chem. Mater. 18 (2006) 2181–2186.
[39] M. Kavitha, R. Subramanian, R. Narayanan, V. Udhayabanu, Solution combustion synthesis and characterization of strontium substituted hydroxyapatite nanocrystals, Powder Technol. 253 (2014) 129–137.
[40] N.D. Thorat, K.P. Shinde, S.H. Pawar, K.C. Barick, C.A. Betty, R.S. Ningthoujam, Polyvinyl alcohol: an efficient fuel for synthesis of superparamagnetic LSMO nanoparticles for biomedical application, Dalton Trans. 41 (2012) 3060–3071.
[41] J. Zhao, X. Dong, M. Bian, J. Zhao, Y. Zhang, Y. Sun, et al., Solution combustion method for synthesis of nanostructured hydroxyapatite, fluorapatite and chlorapatite, Appl. Surf. Sci. 314 (2014) 1026–1033.
[42] N.D. Thorat, S.V. Otari, R.M. Patil, V.M. Khot, A.I. Prasad, R.S. Ningthoujam, et al., Enhanced colloidal stability of polymer coated $La_{0.7}Sr_{0.3}MnO_3$ nanoparticles in physiological media for hyperthermia application, Colloids Surf. B. Biointerfaces 111 (2013) 264–269.
[43] N.D. Thorat, S.V. Otari, R.A. Bohara, H.M. Yadav, V.M. Khot, A.B. Salunkhe, et al., Structured superparamagnetic nanoparticles for high performance mediator of magnetic fluid hyperthermia: synthesis, colloidal stability and biocompatibility evaluation, Mater. Sci. Eng. C. Mater. Biol. Appl. 42 (2014) 637–646.
[44] C.J. Gabelich, T.D. Tran, I.H. "Mel" Suffet, Electrosorption of inorganic salts from aqueous solution using carbon aerogels, Environ. Sci. Technol. 36 (2002) 3010–3019.
[45] S.V. Dorozhkin, A review on the dissolution models of calcium apatites, Prog. Cryst. Growth Charact. Mater. 44 (2002) 45–61.
[46] C. Shi, J. Gao, M. Wang, J. Fu, D. Wang, Y. Zhu, Ultra-trace silver-doped hydrox yapatite with non-cytotoxicity and effective antibacterial activity, Mater. Sci. Eng C55 (2015) 497–550.
[47] N.D. Thorat, S.V. Otari, R.M. Patil, R.A. Bohara, H.M. Yadav, V.B. Koli, et al., Synthesis, characterization and biocompatibility of chitosan functionalized superparamagnetic nanoparticles for heat activated curing of cancer cells, Dalton Trans. 43 (2014) 17343–17351.
[48] R.A. Bohara, N.D. Thorat, H.M. Yadav, S.H. Pawar, One-step synthesis of uniform and biocompatible amine functionalized cobalt ferrite nanoparticles: a potential carrier for biomedical applications, New J. Chem. 38 (2014) 2979.
[49] A.E. Nel, L. Mädler, D. Velegol, T. Xia, E.M.V. Hoek, P. Somasundaran, et al., Understanding biophysicochemical interactions at the nano-bio interface, Nat. Mater. 8 (2009) 543–557.
[50] T. Metanawin, T. Tang, R. Chen, D. Vernon, X. Wang, Cytotoxicity and photocytotoxicity of structure-defined water-soluble C60/micelle supramolecular nanoparticles, Nanotechnology 22 (2011) 235604.
[51] N.D. Thorat, V.M. Khot, A.B. Salunkhe, R.S. Ningthoujam, S.H. Pawar, Functionalization of $La_{(0.7)}Sr_{(0.3)}MnO_3$ nanoparticles with polymer: studies on enhanced hyperthermia and biocompatibility properties for biomedical applications, Colloids Surf. B. Biointerfaces 104 (2013) 40–47.
[52] A.K. Gupta, M. Gupta, Synthesis and surface engineering of iron oxide nanoparticles for biomedical applications, Biomaterials 26 (2005) 3995–4021.